



Comparison of the tissue response of selective retina therapy with or without real-time feedback-controlled dosimetry

Minhee Kim¹ · Young-Gun Park¹ · Seungbum Kang² · Young Jung Roh¹

Received: 20 February 2018 / Revised: 8 May 2018 / Accepted: 12 July 2018 / Published online: 28 July 2018
© Springer-Verlag GmbH Germany, part of Springer Nature 2018

Abstract

Purpose The purpose of this study is to evaluate the retinal tissue response upon selective retina therapy (SRT) with or without real-time feedback-controlled dosimetry (RFD) in rabbits.

Methods Eighteen eyes of nine Chinchilla Bastard rabbits were treated by SRT with or without RFD (Q-switched Nd:YLF, wavelength 527 nm, pulse duration 1.7 μs). RFD operated by optoacoustic and reflectometric methods detects the microbubbles from retinal pigment epithelium (RPE) damage in real time. After SRT, light microscopy (LM) and scanning electron microscopy (SEM) were performed at 1 h, 1 day, 3 days, 7 days, and 1 month. The RPE-damaged area on SEM was measured by ImageJ 1 h after SRT.

Results Without RFD, the RPE-damaged area of 76 SRT-treated spots showed a strong positive correlation with ramping pulse energy (Pearson's correlation coefficient, 0.706; $P < 0.001$). With RFD, there was a weak positive correlation between the RPE-damaged area of 92 spots and ramping pulse energy (Pearson's correlation coefficient, 0.211; $P = 0.044$). The detection rate of RFD was 91.8% by evaluating 563 SRT spots. Histology revealed that SRT with RFD produced a selectively disrupted RPE monolayer while sparing the photoreceptor layer inner segment.

Conclusions RFD can be useful to titrate the pulse energy of visually undetectable SRT treatment.

Keywords Selective retina therapy (SRT) · Real-time feedback-controlled dosimetry (RFD) · Retinal pigmented epithelium (RPE)

Introduction

The value of conventional photocoagulation (PC) is well established in diabetic retinopathy studies [1, 2]. The traditional concept of using PC for retinal vascular disease is to reduce the metabolic burden by destroying the photoreceptors causing the metabolic demand in the ischemic region [3]. However, PC induced serious side effects including central scotoma due to progressive enlargement of laser scarring and choroidal neovascularization [4, 5]. To avoid the side effects, photoreceptor-sparing retinal laser approaches such

as subthreshold (subvisible) diode laser (SDM) and selective retina therapy (SRT) have been used clinically [6–9]. Although the mechanism of photoreceptor-sparing laser is not well understood, the working mechanism is known to be related to the expression of heat shock protein (HSP 70) and matrix metalloproteinases (MMPs) during the healing process [10]. SDM stimulates the RPE monolayer without damaging RPE cells, but on the other hand, SRT does damage RPE cells. Therefore, in addition to releasing bioactive substances during the RPE healing process, the restoration of the RPE monolayer is the basis of the effect of SRT [11]. In addition to the anatomical restoration, recent studies proved that selective RPE damage, in which photoreceptors were spared, did not induce functional loss like scotomatous changes as assessed by electrophysiology and microperimetry [8, 12–14]. While SDM showed favorable results for treating diabetic macular edema (DME), the lack of visibility in the retinal change limits the ability to titer an adequate laser dosage during irradiation. Therefore, SDM pulse energy is adjusted by changing the pulses' "ON/OFF" times (duty cycle) only after observation of SDM spots [7]. A titrating protocol based on endpoint

✉ Young Jung Roh
youngjungroh@hanmail.net

¹ Department of Ophthalmology and Visual Science, Yeouido St. Mary's Hospital, College of Medicine, The Catholic University of Korea, 10, 63-ro, Yeongdeungpo-gu, Seoul 07345, South Korea

² Department of Ophthalmology and Visual Science, Daejeon St. Mary's Hospital, College of Medicine, The Catholic University of Korea, Seoul, South Korea

management (EpM) for achieving reproducible subvisible spots was recently reported [15]. However, titration based on subjective observation for the change in laser spots might run the risk of under- or overtreatment and did not account for intraindividual variance in RPE pigmentation.

While SDM does not induce any retinal tissue damage, SRT damages RPE cells selectively while sparing photoreceptor cells. Selective RPE damage can be achieved by a burst of microsecond micropulses which is mainly absorbed by melanosomes in RPE cells. Microvaporization around melanosomes due to the thermal energy of SRT can cause short-lived microbubbles. However, uncontrolled SRT can cause visible burns on the neurosensory retina if untowardly high energy levels are erroneously used. Therefore, to produce selective RPE damage without photoreceptor damage, two endpoints of SRT spots including invisibility on ophthalmoscopy and visibility on fundus fluorescein angiography (FFA) have been used for SRT treatment [11]. Although SRT treatment based on the pretreating angiographic feature of test spots around major vessel arcades showed promising results for treating DME and CSC, there were several limitations to apply SRT treatment according to the threshold value obtained from test spots. First, although FFA is a useful method to detect RPE damage, undertreatment was occasionally observed at the SRT-treated area due to the anatomical difference between the intact test area and pathologic treatment area with macular edema and subretinal fluid in our previous studies [8, 12]. Second, instant adjustment of pulse energy is mandatory because of inter- or intrapersonal variations in retinal pigmentation. To overcome these limitations, two dosimetric methods were developed to monitor the response of retinal tissue in real time by detecting microbubbles originating from RPE damage. One is optoacoustic (OA) dosimetry which detects the ultrasonic pressure in the form of the optoacoustic feedback value (OAV) originating from microbubbles which occurred around RPE melanosomes during irradiation [16]. The other is the reflectometric (RM) method which detects reflection of backscattered light in the form of the optical feedback reflectometric value (RMV) from transient microbubbles [17]. Although the two dosimetry systems were clinically used in several studies [8, 9, 11, 12], the range of adequate micropulse energy was confirmed only after evaluating angiographic features of test spots. Previously, we demonstrated that real-time feedback-controlled reflectometry was safe and effective in obtaining selective RPE damage in a rabbit experiment [17]. As soon as the ramping micropulse energy reaches the therapeutic threshold which can induce microbubbles, the following burst of micropulses is automatically stopped by reflectometry. Recently, we demonstrated the efficacy of SRT for patients with chronic CSC through real-time feedback-controlled dosimetry (RFD) operated by both OA and RM methods [18].

In this study, RFD with both OA and RM methods was used for the first time to investigate the tissue response in an

animal in vivo experiment. The aim of this study is to investigate the tissue response of the retina and RPE monolayer produced by SRT with or without RFD.

Methods

Animals

Eighteen eyes of 9 Chinchilla Bastard rabbits received selective retina therapy with or without RFD. The animals were anesthetized with zoletil® (Vibrac, Carros, France; 0.2 mg/kg of body weight) and xylazine hydrochloride (5 mg/kg). Topical 0.5% tropicamide and 0.5% phenylephrine hydrochloride (Mydrin-P ophthalmic solution; Santen Pharmaceutical Co., Ltd., Osaka, Japan) were used for dilating the pupils. The rabbits in this experiment were treated in accordance with the ARVO Statement for the Use of Animals in Ophthalmic and Vision Research, and were approved by the Institutional Animal Care and Use Committee of the Catholic University of Korea.

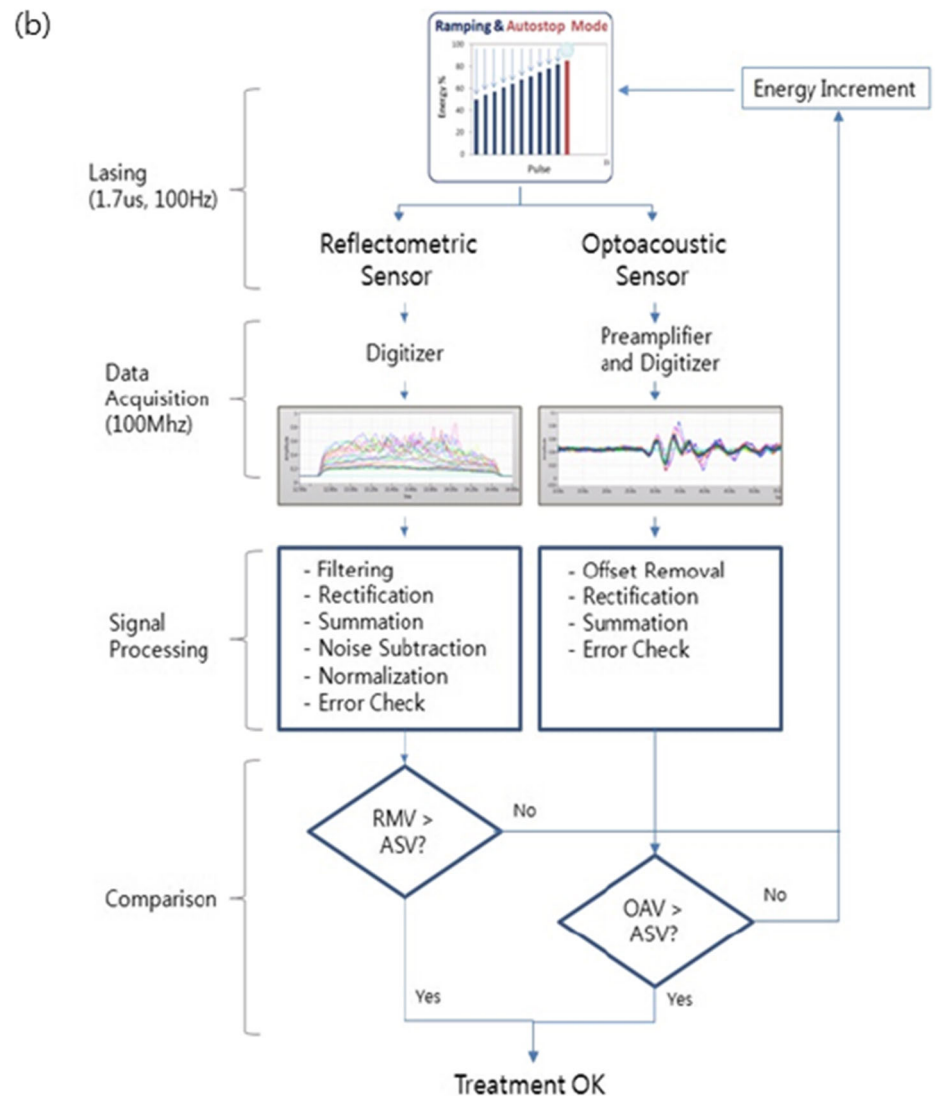
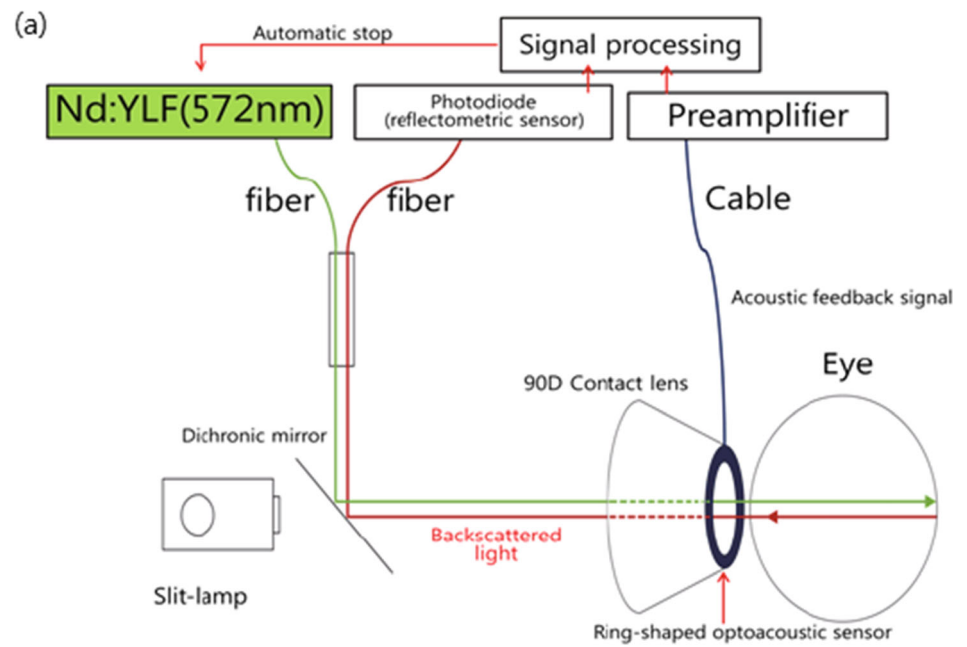
Selective retina therapy setup and laser irradiation

The animals were treated with a SRT Laser system (R:GEN, Lutronic, Goyang-si, South Korea), Q-switched Nd:YLF laser: wavelength, 527 nm; pulse duration, 1.7 μ s; repetition rate, 100 Hz. The laser system delivers 15 micropulses in a burst of stepwise ramping micropulse energies. The last (15th) micropulse energy (LPE) can be adjusted by the clinician as a preset pulse energy. The first pulse energy is 50% of the LPE, and the energy of the following micropulses is increased by additional 3.57%.

As the pulse energy of the laser is raised, the temperature of the melanosome surfaces in the laser spot area increases and microbubbles are generated. These microbubble signals can be monitored with the OA and RM sensors. For OA signal measurement, a ring-shape piezoceramic sensor is embedded in the contact lens (field of view, 90D; image magnification, \times 1.05; Lutronic, South Korea) placed on the rabbit's eye (Fig. 1a). The detected signal in the frequency range of 20 kHz to 2 MHz is processed as can be seen in Fig. 1b below. The final outcome of the processing is measured as the OAV, an arbitrary value. The implemented OA algorithm employs the OA signal from microbubble formation to discriminate from those OA signals originating from thermo-elastic expansion of the tissue without bubble formation. Thus, OAV can be seen as a processed barometer of the acoustic energy originating from the RPE cells, and any OAV above the predetermined value is considered as exceeding the damage threshold in RFD.

The RM signal is obtained by measuring the scattered laser signal from the microbubbles. The process of the detected

Fig. 1 a The setup of real-time feedback-controlled dosimetry (RFD). A photodiode was used as a reflectometric (RM) sensor to acquire backscattered light. Acoustic transients were detected by a contact lens with an inserted ring-shaped piezoceramic optoacoustic (OA) sensor. **b** A schematic diagram showing the signal processing of RFD with OA and RM sensors. RMV reflectometric value, OAV optoacoustic value, ASV autostop value



signal is shown in Fig. 1. The final outcome of this process is measured as the RMV, which is also an arbitrary value. Like the OAV, the RMV is considered to be above threshold as soon as it exceeds the predetermined value.

The feedback of OA and RM signals from microbubble formation considers there is RPE cellular damage when either of the feedback signals is above the threshold after each individual laser micropulse is delivered. As soon as the threshold was obtained by detecting microbubble formation, the subsequent burst of micropulses was automatically stopped by the laser system based on an “OR” relationship between OA and RM. The individual micropulse energy among 15 micropulses producing autostop due to selective RPE damage is referred to as the selective micropulse energy (SMPE).

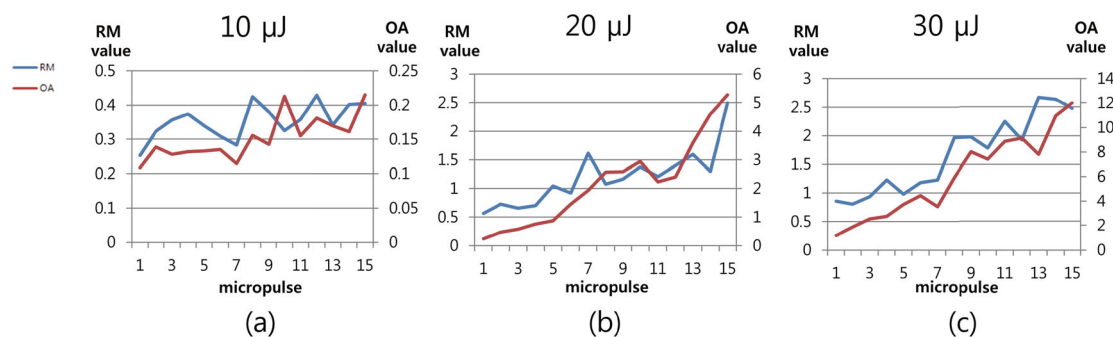
By changing the software and the laser pulse energy, the SRT system designed for humans was adjusted for rabbits in this study. The modified algorithm of RFD for animal subjects (RFD-val.1.1) was used due to the differences in the range of pulse energy for selective RPE damage between human (60–200 μJ) and rabbit (11–48 μJ)

eyes [8, 9, 16, 17]. Although the basic algorithm of RFD for rabbit eyes is the same as for humans, the limit of minimum output laser energy level was lowered to 5 μJ for this study.

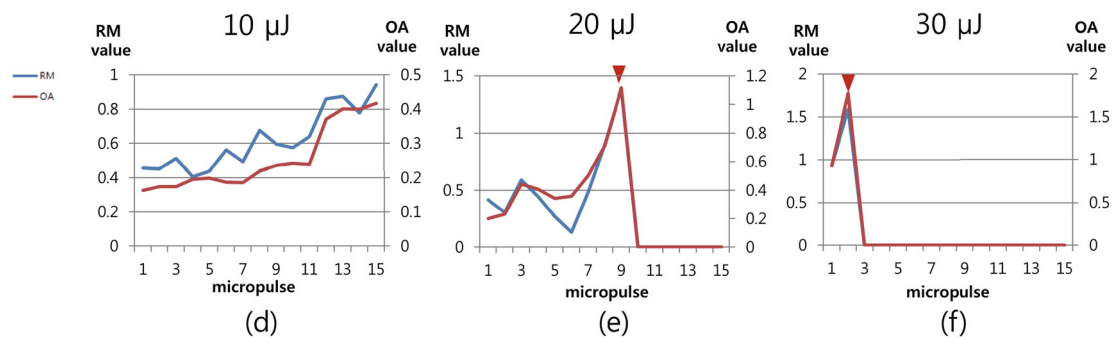
Since the OA and RM values that demonstrate damage in rabbit RPE cells are different from those for human beings, the threshold values stored in the algorithm were also modified before the experiment. The criterion value used as the bubble formation threshold in this rabbit experiment is obtained by comparing the OAV and RMV with FFA image for each respective SRT spot.

The placement of autostop among 15 micropulses was recorded when the rabbits were treated by SRT with RFD. In addition, the feedback signal from SRT without RFD was also recorded to compare the pattern of feedback signal with or without RFD. As the pulse energy increases during treatment, there is a tendency for more RPE cells to become damaged. However, OAV and RMV increase irregularly because of their own noise component and different signal change gradient (Fig. 2).

Without RFD



With RFD



RFD, real-time feedback-controlled dosimetry; RM, reflectometric; OA, optoacoustic

Fig. 2 The laser pulse energy of selective retina therapy (SRT) is increased with every micropulse by an additional 3.57% of the dynamic range. **a–c** Without RFD, each feedback signal of OA and RM dosimetry increases as the micropulse energy is increased stepwise. **d–f** With RFD, laser irradiation was stopped as soon as the feedback signal, the calculated quantification of modulations, reached the threshold level (red arrowhead). The threshold values of OA and RM dosimetry were set to

1.0 and 1.2 arbitrary units (AU) respectively. **e** Since autostop occurred at the 10th micropulse during 20 μJ SRT irradiation with RFD by the feedback of OA and RM dosimetry, selective micropulse energy (SMPE) is the 9th micropulse (SMPE, 15.7 μJ). **f** In the case of 30 μJ laser irradiation, autostop occurred at the 3rd micropulse (SMPE, 16.1 μJ) by OA and RM dosimetry

Selective retina therapy protocol

The two endpoints of “adequate” SRT spots were defined as invisible on ophthalmoscopy, but visible on FFA in a previous study [11]. Based on the protocol, six eyes were treated by SRT without RFD, eight eyes with RFD, and the remaining four eyes were treated by SRT with and without RFD (Table 1). To provide orientation for the invisible SRT irradiation and tissue pathology, the marker lesions (100–140 μJ) were initially applied one disc diameter beneath the optic nerve head along the horizontal medullary ray using the SRT without RFD. Then, SRT spots with or without RFD were placed along these marker burns in the inferior parapapillary retina and were documented graphically. SRT spots (48–72 spots) were placed in each eye with a range of 5–45 μJ . The minimum angiographic threshold energy was defined from the preset LPE of SRT spot for each eye (Table 1).

In vivo imaging

To evaluate the ophthalmoscopic and angiographic threshold, color fundus photography (CFP) and FFA (TRC-50DX, Topcon Corp., Tokyo, Japan) were performed in all rabbits 1 h after treatment. CFP and FFA were repeated in rabbit no. 9, 1 month after SRT.

Since SRT spots are invisible during irradiation on ophthalmoscopy, instant visible changes in the SRT spots were

regarded as a burn. When invisible SRT spots during irradiation changed to “barely visible” spots on CFP 1 h after SRT, the spots were considered as “adequate” SRT spots because the spots eventually became invisible on both FFA and CFP in our previous study [8, 17]. Therefore, invisible and delayed barely visible spots were classified as adequate SRT spots.

Light microscopy and scanning electron microscopy

The animals were sacrificed by injection of an overdose of KCL, and eyes were enucleated for histology 1 h, 1 day, 3 days, 7 days, and 1 month after treatment (Table 1). By using the optic nerve head, inferior medullary rays and marker burns as landmarks, tissue pathology was performed to include both marker and SRT lesions. Tissue specimens were routinely prepared for staining with hematoxylin and eosin for histological analysis as previously described [17]. SEM was performed in the other eyes to observe the area of RPE damage 1 h, 1 day, 3 days, 7 days, and 1 month after treatment. The posterior eye cup was incised from the anterior segment of the globe and the posterior part was immersed in saline solution for 30 min and then the retina was manually peeled from the RPE. The remaining tissues including sclera, choroid, and RPE were fixed in 2.5% glutaraldehyde in 0.1 M phosphate buffer (pH 7.4) for 2 h at 4 °C. After rinsing several times in a buffer, they were postfixed

Table 1 Summary of rabbit eyes used in this study

Rabbit no.	OD/OS	Total no. of SRT spots (with RFD, without RFD)	Time of histologic exam after SRT treatment	Minimum angiographic threshold energy from SRT spots (μJ)	The range of preset LPE of SRT spots (μJ)
1	OD	50 (0.50)	1 h (LM)	5	5, 10, 15, 20, 25
	OS	50 (0.50)	1 h (SEM)	5	5, 10, 15, 20, 25
2	OD	50 (0.50)	1 h (SEM)	10	5, 10, 15, 20, 25
	OS	50 (0.50)	1 h (LM)	10	5, 10, 15, 20, 25
3	OD	54 (0.54)	1 h (LM)	10	5, 10, 15, 20, 25
	OS	54 (0.54)	1 h (SEM)	10	5, 10, 15, 20, 25
4	OD	54 (54.0)	1 h (LM)	10	10, 20, 30
	OS	54 (54.0)	1 h (SEM)	10	10, 20, 30
5	OD	50 (50.0)	1 h (SEM)	10	10, 20, 30
	OS	50 (50.0)	1 h (LM)	10	10, 20, 30
6	OD	48 (48.0)	1 day (LM)	5	5, 10, 20, 30
	OS	48 (48.0)	1 day (SEM)	5	5, 10, 20, 30
7	OD	48 (36.12)	3 days (SEM)	10	10, 20, 30
	OS	48 (36.12)	3 days (LM)	10	10, 20, 30
8	OD	50 (40.10)	7 days (LM)	15	15, 25, 35, 45
	OS	72 (54.18)	7 days (SEM)	15	15, 25, 35, 45
9	OD	51 (51.0)	1 month (LM)	15	15, 25, 35, 45
	OS	50 (50.0)	1 month (SEM)	15	15, 25, 35, 45

SRT selective retina therapy, RFD real-time feedback-controlled dosimetry, LM light microscopy, SEM scanning electron microscopy, LPE the last (15th) micropulse energy

with 2% osmium tetroxide for 2 h at 4 °C and then the tissue was washed with distilled water. After standard dehydration in an ethanol series, the samples were freeze-dried (Hitachi ES-2030, Tokyo, Japan) and coated with platinum in an ion coater (Eiko IB-5, Tokyo, Japan) for SEM observation (Hitachi S-4700, Tokyo, Japan). The area of RPE damage 1 h after SRT with or without RFD was outlined and measured using ImageJ (NIH, Bethesda, MD, USA). The pixels of the RPE-damaged area were measured by using the image with scale bar. Then, the pixels were converted to the scale “ μm^2 .”

Results

Ophthalmoscopic examination and fundus fluorescein angiography

Without RFD, all SRT spots ($\geq 25 \mu\text{J}$) showed visible change on retina during irradiation in all rabbits. However, with RFD, no instant visible spots on ophthalmoscopy were observed with a range of 5–45 μJ in this study. Without RFD, a total of 308 SRT treatment spots were created for 6 eyes of rabbit nos. 1–3 by increasing pulse energies including 5, 10, 15, 20, and 25 μJ respectively. While no visible change was observed at $\leq 20 \mu\text{J}$ spots during irradiation, instant visible change like a burn was observed at 25 μJ spots during irradiation. Some of the invisible 10, 15, and 20 μJ SRT spots during irradiation changed to “barely visible” spots on CFP 1 h after SRT (Fig. 3a). FFA demonstrated hyperfluorescence in all $\geq 10 \mu\text{J}$ SRT spots produced by SRT without RFD. Although all of the 5 μJ spots in rabbit nos. 2 and 3 showed no hyperfluorescence, all of the 5 μJ spots in rabbit no. 1 showed relatively faint hyperfluorescence compared to other $\geq 10 \mu\text{J}$ spots. The minimum angiographic threshold of SRT spots of each rabbit was either 5, 10, or 15 μJ after evaluating all SRT spots on FFA (Table 1). All 25 μJ spots without RFD showed instant visible changes like burns and were considered as overtreatment. With RFD, a total of 571 SRT spots were irradiated for 12 eyes of rabbit nos. 4–9. While some “barely visible” spots were observed on CFP obtained 1 h after SRT with 30 μJ or above (Fig. 4a), all SRT spots with RFD demonstrated no instant visible changes during irradiation.

Scanning electron microscopy

The damaged RPE cells in the center of SRT spots were observed on SEM 1 h after SRT with or without RFD. Although coagulated and destroyed retinal tissue was shown at the marker burn on SEM images, SRT lesions revealed a well-delineated area of RPE damage without breaks of Bruch’s membrane (BM) (Figs. 3b and 4b). Since the profile of the laser beam coming out of the multimode

optical fiber with a 50- μm core diameter is no longer Gaussian, the shape of the RPE-damaged area is not round with a smooth edge. Above the threshold energy, the RPE-damaged area by SRT without RFD showed a strong positive correlation with ramping pulse energy when 76 SRT spots were analyzed in three eyes of rabbit nos. 1–3 (Pearson’s correlation coefficient, 0.706; $P < 0.001$) (Fig. 3e). The mean \pm SD RPE-damaged area ($15,699 \pm 4652 \mu\text{m}^2$) by SRT without RFD was higher than the SRT-irradiated area ($15,386 \mu\text{m}^2$). After SRT with RFD, there was a weak positive correlation between the RPE-damaged area of 92 spots and ramping pulse energy (10–30 μJ) in two eyes of rabbit nos. 4 and 5 (Pearson’s correlation coefficient, 0.211; $P = 0.044$) (Fig. 4c). The mean RPE-damaged area ($13,462 \pm 1300 \mu\text{m}^2$) by SRT with RFD was lower than the SRT-irradiated area. On SEM 1 day after SRT with RFD, SRT lesions showed a migration of RPE cells at the margin of the damaged area (Fig. 5b). Some of the SRT lesions showed attached outer photoreceptor segments (Fig. 5c). Furthermore, SRT lesions were mostly covered by migration and proliferation of adjacent RPE cells by 3 days (Fig. 6b). Although 30 μJ spots without RFD were visible on ophthalmoscopy, 30 μJ spots with RFD were invisible in the same eye. This result demonstrates that RFD can prevent overtreatment effectively regardless of intraindividual variation of RPE pigmentations in the same eye. On SEM 7 days after SRT, most of the damaged areas were fully covered by an increased density of smaller RPE cells (Fig. 6c). Following the restoration of the RPE monolayer, SRT spots were hardly distinguishable from adjacent healthy RPE cells. On SEM 1 month after SRT with RFD, the SRT lesions could not be differentiated from adjacent untreated regions because of complete RPE rejuvenation with increased density of RPE cells (Fig. 7e).

Light microscopy

No change was observed in RPE monolayers and photoreceptor layers on LM 1 h after SRT (Fig. 4d). Focal proliferated RPE cells with a relaxed photoreceptor outer segment were observed at SRT spots 1 day after SRT with RFD (Fig. 5d). The marker burns showed a full thickness distortion of retinal tissue and multiple proliferated RPE cells in the inner retina layer after 3 days and SRT with RFD spots showed focal proliferated RPE cells with sparing of photoreceptor cells (Fig. 6d). After 7 days, single- or double-layered RPE cells were observed at the SRT with RFD lesions without distortion of the photoreceptor inner segment and inner retinal layer (Fig. 6e). On LM after 3 days, double marker burns were used to navigate the row of SRT lesion without RFD to differentiate from spots with RFD (Fig. 6f). On LM 1 month after SRT,

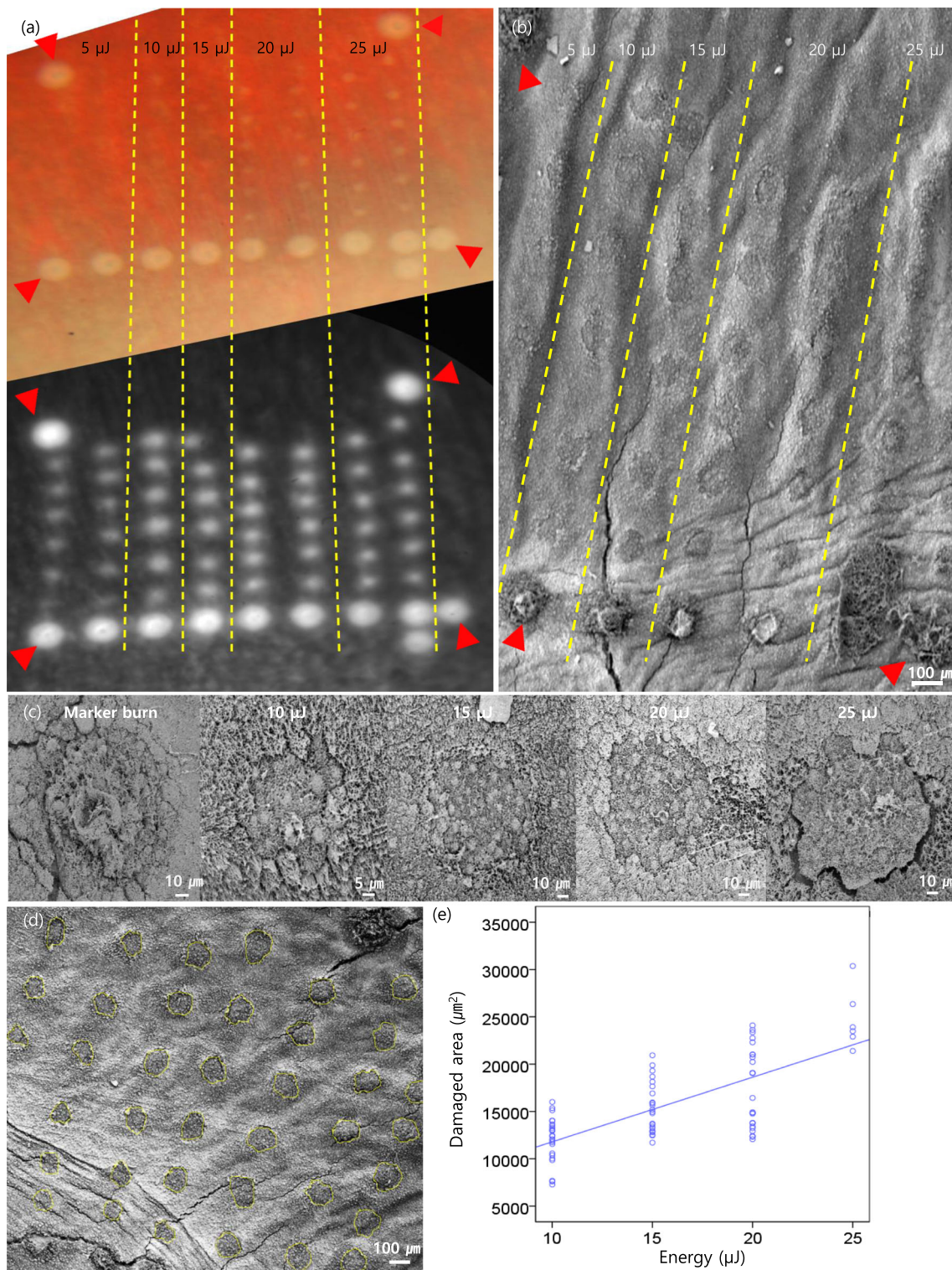


Fig. 3 The tissue reaction 1 h after SRT without RFD. **a** Color fundus photography (CFP) 1 h after SRT without RFD shows invisible (5, 10 μJ spots), barely visible (10, 15, 20 μJ) and visible lesions (25 μJ). Whitish marker burns (red arrowhead) are observed. Although the spots with 10, 15, and 20 μJ are originally invisible lesions, some of spots changed to “barely visible” lesions 1 h after SRT. One hundred percent of 25 μJ SRT spots show visible changes instantly. Although invisible 5 μJ SRT spots on ophthalmoscopy show faint hyperfluorescence on fundus fluorescein angiography (FFA) 1 h after SRT, all other spots (10, 15, 20, 25 μJ) show significant hyperfluorescence. **b** Scanning electron microscopy (SEM) of

RPE 1 h after SRT without RFD. Marker lesions (red arrowhead) show coagulated and destroyed retinal tissues. **c** SEM of 10, 15, and 20 μJ SRT lesions reveal RPE damage without breaking Bruch’s membrane and show a tendency towards enlarged damaged areas concomitantly with increasing pulse energy. A 25 μJ SRT spot lesion shows wider RPE damage and debris of photoreceptor outer segments. **d** The damaged area of the RPE monolayer by SEM is measured with ImageJ. **e** The RPE-damaged area by SRT without RFD shows a strong positive correlation with increasing pulse energy (10–25 μJ) (Pearson’s correlation coefficient, 0.706; $P < 0.001$)

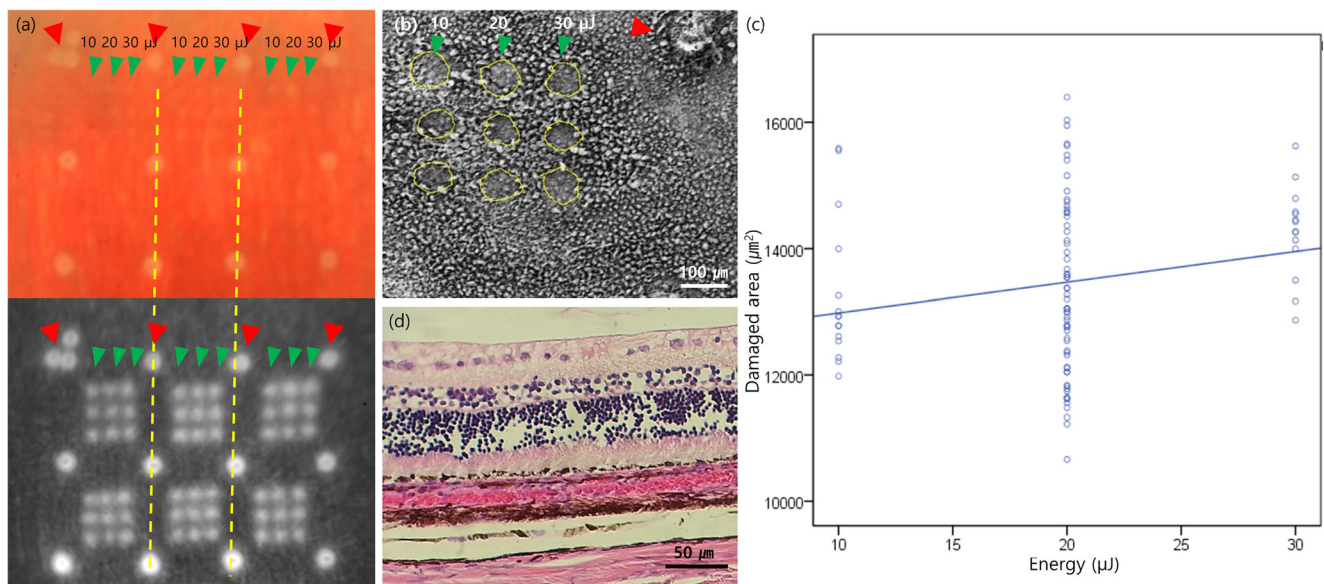


Fig. 4 The tissue reaction at SRT spots 1 h after SRT with RFD. **a** CFP 1 h after SRT with RFD shows invisible (10, 20 μJ spots) or barely visible SRT lesions (some of 30 μJ spots) between whitish marker burns (red arrowhead). Although all SRT spots (green arrowhead) were invisible lesions during irradiation, 35% of spots have changed to barely visible lesions 1 h after SRT. No instantly visible spots were observed during irradiation. FFA shows significant hyperfluorescence of SRT spots (green arrowhead) between stronger hyperfluorescence of marker lesions

(red arrowhead). **b** SEM of RPE 1 h after SRT with RFD. The damaged area was measured with ImageJ. SRT lesions (yellow dotted circle) reveal damaged RPE cells in the center of SRT spots. **c** The RPE damaged area by SRT with RFD shows a weak positive correlation with increasing pulse energy (10, 20, 30 μJ). (Pearson's correlation coefficient, 0.211; $P=0.044$). **d** No photoreceptor and Bruch's membrane damage is seen on light microscopy (LM) 1 h after SRT

except for the focal proliferated RPE cells, SRT lesions were almost indistinguishable from the untreated RPE monolayer (Fig. 7g).

Real-time feedback-controlled dosimetry

The OAV and RMV of SRT spots with (563 spots) or without RFD (178 spots) were analyzed after excluding 8 SRT spots with RFD due to defocusing error occurred by sudden movement of rabbit. Without RFD, OAV and RMV increased simultaneously with the ramping micropulse energy. Although the lowest OAV and RMV of visible SRT spots like burns on CFP and FFA were approximately 2.0 AU and 1.4 AU respectively, 46 of 48 (95.8%) visible spots on CFP showed above 8.0 AU of OAV or 2.2 AU of RMV (Fig. 8a). Therefore, the threshold of RFD-va1.1 (OAV 1.0 AU, RMV 1.2 AU) was deemed to have an adequate margin of safety. In the rabbits treated by SRT with RFD (rabbit nos. 4–9), the autostop occurred in 470 of 563 spots when the ramping micropulse energy (10–45 μJ) reached the predetermined threshold. The ratio of the number of adequate SRT spots above the threshold of OA or RM to the number of all FFA-visible spots indicates the detection rate of RPE damage by RFD. The detection rate of RFD using OA or RM was 91.8% (470/512 spots) by evaluating 563 SRT spots. The detection rate of each OA and RM was 88.6% (454/512 spots) and 48.6% (249/512 spots) respectively. Although 42 of 93 spots showing no-autostop demonstrated FFA-positive spots, no overtreatment

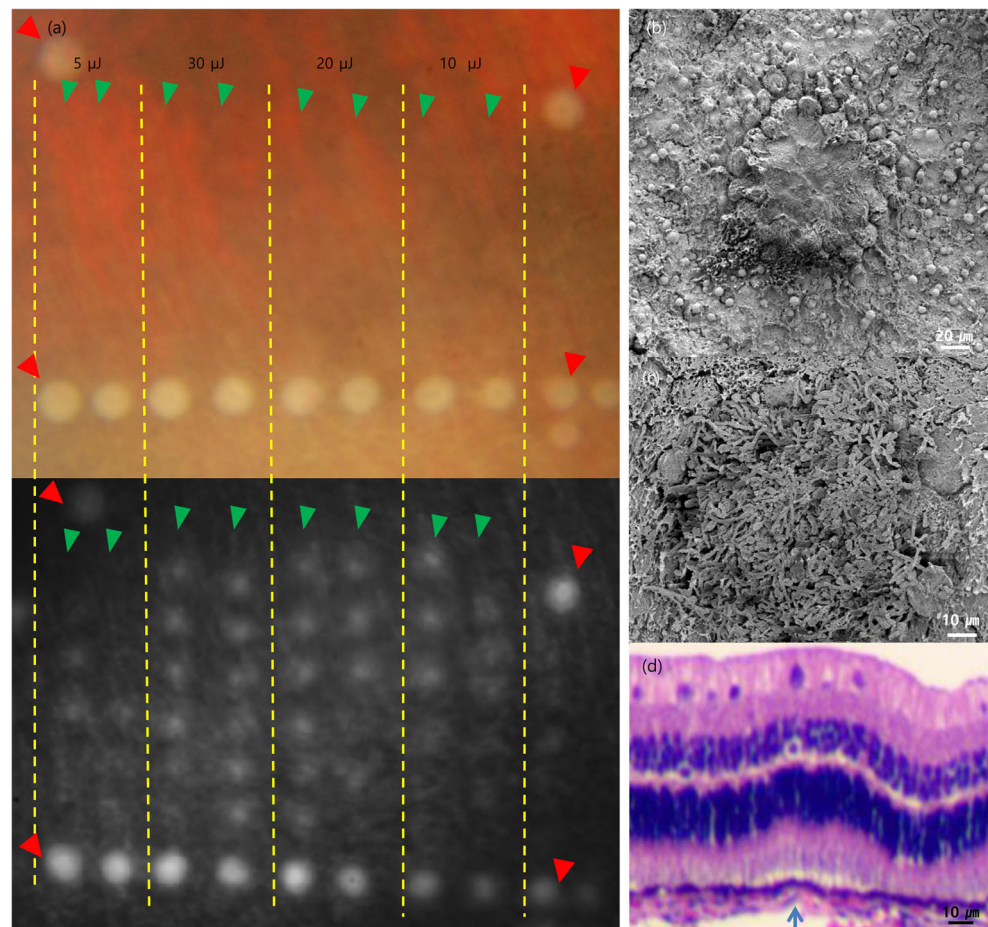
like burns was observed (Fig. 8b). Since the autostop happened in between the 1st and 15th micropulse during microbursts, the mean real-applied pulse energy of the SMPE was less than the mean preset LPE in rabbit nos. 4–9 (Fig. 8c).

Discussion

Because of the invisibility of SRT and SDM lesions during irradiation, several methods of titrating the pulse energy have been developed to find the adequate pulse energy. For titration of SDM, the fixed parameter like the lowest duty cycle (5%) was used in a clinical study [19]. A new titrating procedure of EpM titers the pulse energy by a percentage of the 100% EpM setting which results in a minimally visible retinal lesion [15]. Based on the EpM protocol, tissue damage at <30% energy level was classified as non-damaging photostimulation with single visible RPE damage. However, >50% energy level of the EpM setting demonstrated the partial loss of nuclei in the outer nuclear layer. In terms of the endpoint of SRT-like selective RPE damage, <30% and >50% energy levels can be respectively classified as undertreatment and overtreatment. Therefore, pulse energy adjustment based on a fixed parameter such as duty cycle and percentage titration is difficult to apply to acquire the endpoints of SRT.

Since two endpoints including invisibility of SRT spots on ophthalmoscopy and visibility on FFA are clinically applied for selective RPE damage, the OA and RM methods for SRT

Fig. 5 The tissue reaction 1 day after SRT with RFD. **a** A CFP 1 h after SRT with RFD shows invisible or barely visible lesions between whitish marker burns (red arrowhead). Although all SRT spots are invisible lesions during irradiation, some barely visible lesions are observed in 30 μ J spots 1 h after SRT treatment. FFA shows visible hyperfluorescence of SRT spots with ≥ 10 μ J. Some of the 5 μ J spots show a faint hyperfluorescence in the absence of autostop. **b** SEM of RPE 1 day after SRT with RFD. The area of the SRT-treated region was variable due to inconsistent migrating of RPE cells 1 day after SRT. The magnified image of SRT lesions reveals migration beginning at the margin of the SRT-treated area of Bruch's membrane. **c** SEM of some "barely visible" lesion shows attached photoreceptor outer segment. **d** LM shows selective RPE damage with a relaxed photoreceptor outer segment (blue arrow) 1 day after SRT. The photoreceptor inner segments have been spared



have been developed to obtain selective RPE damage regardless of inter- or intrapersonal variation of retinal pigmentation and to find the therapeutic threshold without performing invasive FFA.

To detect the development of microbubbles originating from RPE damage in real time, OA and RM methods monitor feedback signals from microbubbles in the form of OAV and RMV, respectively. In the previous studies, by evaluating the correlation between angiographic features of SRT spots and the feedback value, the sensitivity and specificity of OA device were 86 and 70% respectively, and the sensitivity and specificity of RM device were 89 and 94% respectively [8, 9]. RFD using OA and RM devices simultaneously was therefore adopted to improve accurate dosimetry in the current study.

The tissue response of SRT with or without RFD was evaluated over 1 month based on the RFD-v1.1 algorithm. Without RFD, the feedback signals from OA and RM dosimetry increased with increased preset pulse energy (Fig. 2a–c). With RFD, as soon as the feedback signal reached the threshold level at which microbubbles occurred in the RPE (arrowhead), the irradiation of the following micropulse was stopped

automatically (Fig. 2d–f). As the feedback signal reached the threshold, both OAV and RMV simultaneously approached the threshold values, indicating that the two dosimetric feedback approaches were well in synchrony (Fig. 2e, f). However, the RFD system was designed to work in an “OR relation” between OA and RM methods because the OAV and RMV reached the threshold value asynchronously in many SRT spots. Without RFD, all ≥ 25 μ J SRT spots in rabbits (nos. 1–3) showed instant discoloration during irradiation (Fig. 3a). However, with RFD, no SRT spots showed instant whitening like a marker burn (Figs. 4a, 5a, 6a, and 7a). The area of RPE damage on SEM was measured 1 h after SRT to exclude healing process-associated confounding factors. Without RFD, the damaged RPE monolayer area 1 h after SRT showed a strong positive correlation with the increase of the pulse energy (10–25 μ J) (Fig. 3e). With RFD, the damaged area of RPE monolayer showed a weak positive correlation with the ramping pulse energy (10–30 μ J) (Fig. 4c).

Since the 1st micropulse of preset LPE of SRT spots starts at the 50% of the preset LPE, the 1st micropulse proportionally is increased according to the increment of preset LPE. In this study, we evaluated the safety of SRT by applying SRT spots with 200–300% of minimum angiographic threshold in

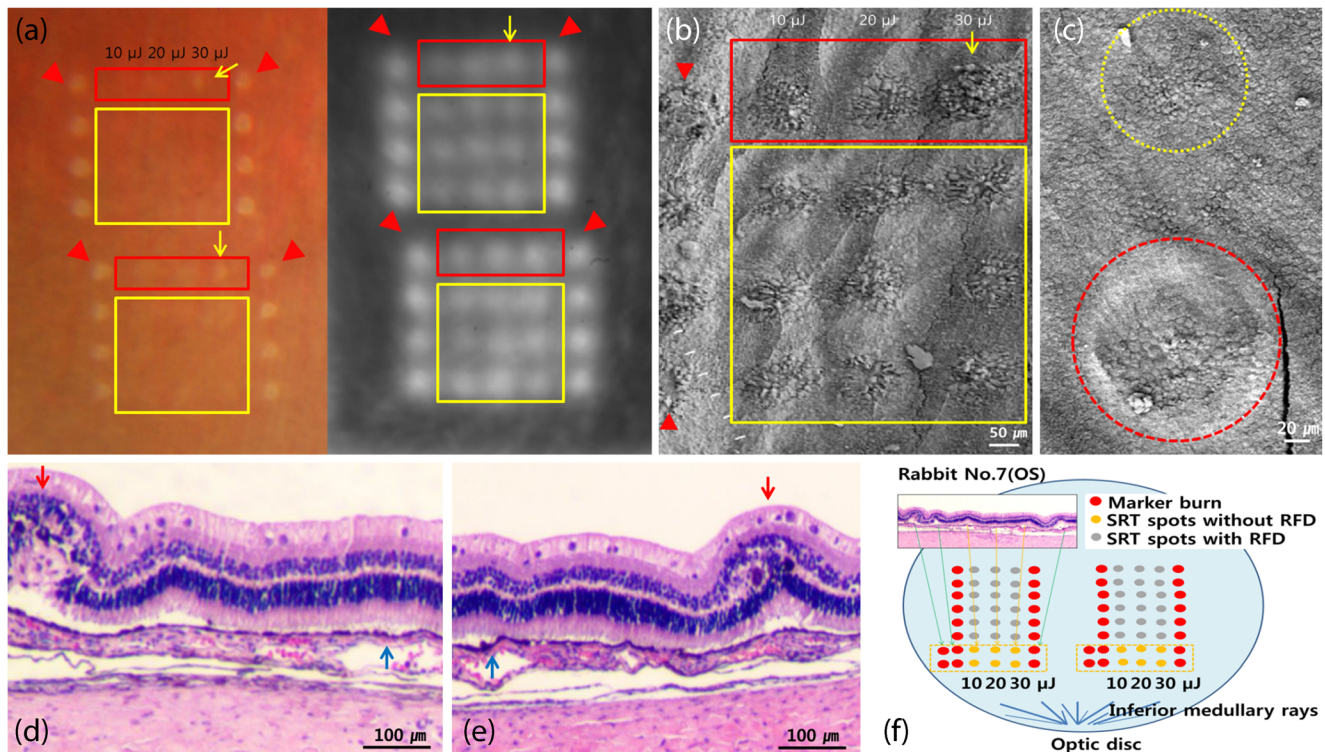


Fig. 6 The tissue reaction 3 days with or without RFD and 7 days after SRT with RFD. **a** CFP 1 h after SRT with RFD (yellow square) shows invisible SRT lesions at 10, 20, and 30 μJ of pulse energy. Whitish marker burns (red arrowhead) are observed. Without RFD (red square), SRT spots (30 μJ) produced instant visible burns (yellow arrow). **(b)** SEM of RPE 3 days after SRT with or without RFD. While SRT without RFD (red square) has produced coagulated and destroyed retinal cells like marker burns at 30 μJ of pulse energy (yellow arrow), SRT lesions with RFD reveal restoration of the RPE monolayer by an increased density of smaller RPE cells (yellow square) with a less hexagonal shape. **(c)** SEM shows that the SRT-damaged area has been fully covered by an increased number of smaller RPE cells 7 days after SRT with RFD. Well-defined marker burns (red circle) show scarce RPE cells without breaks of

Bruch's membrane, whereas the SRT-treated area (yellow circle) is almost indistinguishable from the adjacent untreated area because of restoration of the RPE monolayer. **(d)** LM shows full thickness retinal tissue damage at the marker burns (red arrow) and demonstrates focal RPE proliferation with a relaxed outer segment of photoreceptor layer at SRT lesions with RFD (blue arrow) 3 days after SRT. **(e)** LM shows focal proliferated RPE cells and a spared photoreceptor layer at SRT spots with RFD (blue arrow) and demonstrates distorted retinal tissue and abnormally located multiple pigmented RPE cells in the inner retina at marker burns (red arrow) 7 days after SRT. **(f)** SRT treatment protocol of rabbit no. 7. Double marker burns are used to differentiate the SRT spots without RFD from the SRT spots with RFD 3 days after SRT

the range of high preset LPE, which frequently led to early autostops such as the 1st or 2nd micropulse. Therefore, we speculate that a weak positive correlation might be related with the increasing pulse energy of 1st micropulse. Therefore, these results support the efficacy of RFD to produce similar autostop-controlled RPE damage regardless of ramping pulse energies. Although some invisible SRT spots changed to “barely visible” lesions on CFP 1 h after SRT, the spots were classified as “adequate” SRT spots because the “barely visible” lesions were not related with photoreceptor damage in our previous study [8, 17]. LM and SEM did not reveal any distortion of the photoreceptor layer and BM in all SRT with RFD spots in this study (Figs. 4, 5, 6, and 7). SRT-treated lesions showed the increased density of smaller RPE cells and less hexagonal patterns (Fig. 7e). Therefore, RPE restoration by SRT with RFD was completed by 7 days histologically, which is similar to the tissue response of SRT controlled by pretreatment angiographic findings [11, 13, 17]. Since histology was performed in only

one rabbit 1 month after SRT, the confirmation of the long-term effect of SRT with RFD is, however, limited.

Among 93 spots that showed no autostop, 42 spots demonstrated faint FFA-positive spots due to smaller RPE damage [17, 20]. These spots were in the range of minimum angiographic threshold, 5–10 μJ , which obstructed RFD from detecting RPE damage as the RFD-va1.1 was originally set to above meridian effective dose (ED50) threshold for angiographic visibility. However, all 571 SRT with RFD spots showed no instant visible changes on ophthalmoscopy like burns; thus, the threshold of RFD-va1.1 (OA; 1.0 AU, RM; 1.2 AU) might have an adequate margin of safety for rabbits. While the accuracy of dosimetry was presented by the value of specificity and sensitivity in the previous studies, the detection rate of dosimetry could be a useful value to check SRT spots without performing FFA. In this study, the detection rate of RFD (91.8%)

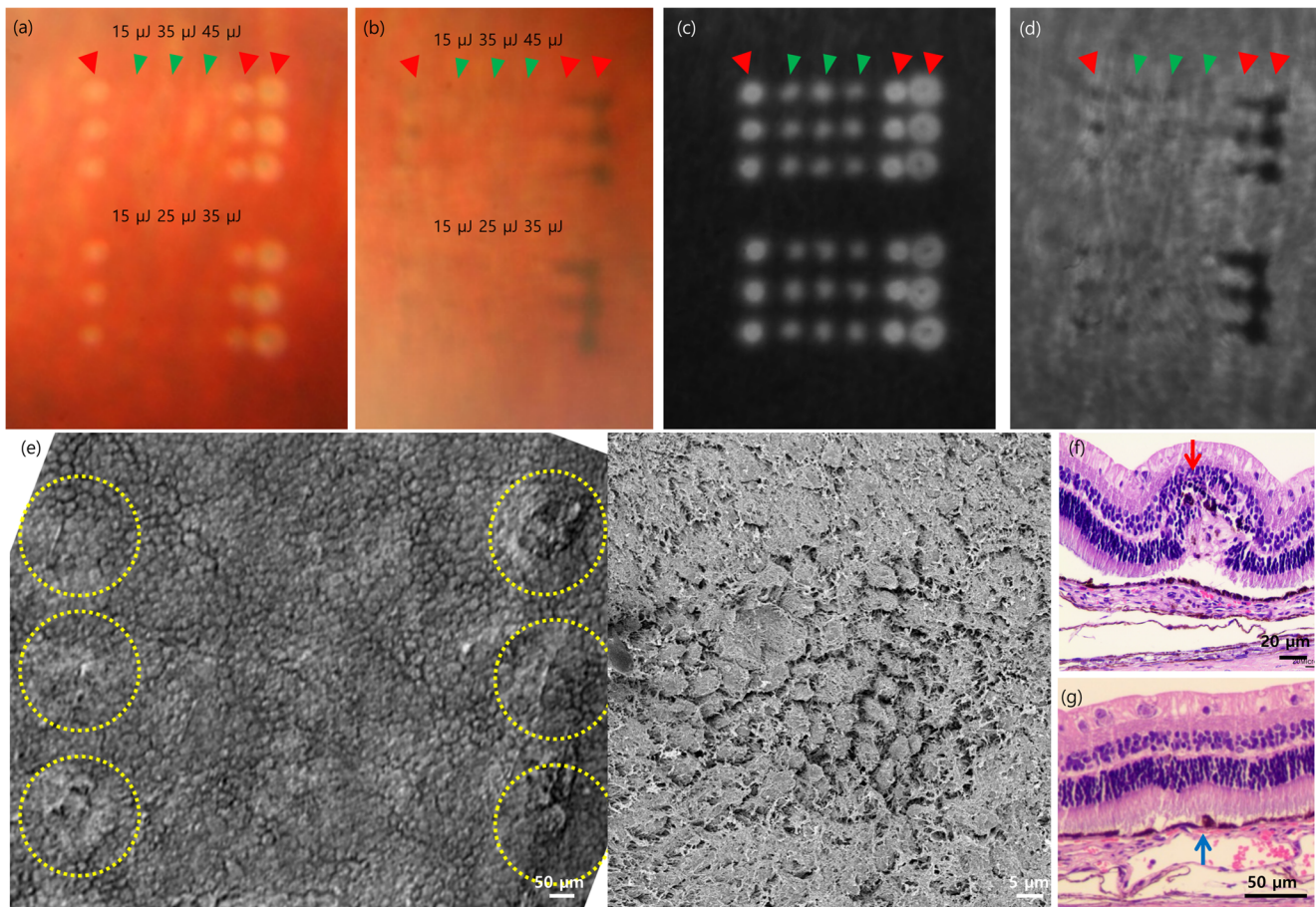


Fig. 7 The tissue reaction 1 month after SRT with RFD. **a** CFP 1 h after SRT with RFD shows invisible (15, 25, 35 μ J spots) and barely visible (45 μ J spots) SRT lesions. Whitish marker burns (red arrowhead) are observed. SRT spots have produced invisible lesions (green arrowhead). **b** Significant pigmentation of marker lesions is observed, but focal pigmented SRT lesions are seen 1 month after laser irradiation. **c** FFA 1 h after SRT demonstrates hyperfluorescence at SRT spots (green arrowhead) and marker lesions (red arrowhead). **d** FFA 1 month after laser treatment shows blocked fluorescence due to thick pigmentation at marker lesions and demonstrated blocked fluorescence due to focal pigmentation at SRT lesions. **e** SEM of RPE monolayer 1 month after

SRT with RFD. While marker lesions (yellow circle) reveal the well-defined destroyed retinal tissues, SRT lesions are indistinguishable from the adjacent untreated area because of restoration of the RPE monolayer. The increased number of smaller RPE cells at the center of SRT lesion show less hexagonality than adjacent untreated RPE cells (left image). The magnified image shows an increased number of smaller-sized RPE cells at the SRT-treated region (right image). **f** LM demonstrates full thickness retinal tissue damage at the marker burns (red arrow). **g** LM shows focal RPE proliferation with spared photoreceptor layer at SRT lesions (blue arrow)

using both OA and RM was slightly improved compared to that of OA alone (88.6%). Therefore, OA worked much better than RM because the number of spots stopped by only RM (16 spots within the left upper quadrant) was smaller than those stopped by OA (221 spots within the right lower quadrant) (Fig. 8b). Even though OA detected RPE damages faster than RM for most of the spots within the right lower quadrant in this study, OA and RM can work complementarily as some spots are detected only by OA or RM. If the threshold of RM is lowered from 1.2 to 1.0 AU, the detection rate of RM is increased from 48.6 to 70.1% by detecting additional 110 spots. Therefore, the detection rate of RFD can be improved by optimizing OA and RM.

Since the mean real-applied pulse energy was lower than the preset LPE in all eyes of rabbits after SRT with

RFD (Fig. 8c), autostop by OA and RM was effective for preventing overtreatment. Even though 45 μ J SRT spots did not induce instant discoloration, about 80% of 45 μ J spots showed “barely visible” SRT with RFD spots on CFP 1 h later. Considering that the minimum pulse energy is 50% of LPE, SMPE (the real-applied pulse energy) is 22.5 μ J when autostop happens right after the 1st micropulse of 45 μ J spots. Therefore, SMPE (22.5 μ J) of all 45 μ J spots were within the range of angiographic threshold (≥ 15 μ J, < 25 μ J), demonstrating no burns.

Since RFD can provide real-time feedback signals showing the placement of autostop, the clinician can adjust the preset LPE instantly to avoid under- or overtreatment. However, the creation of test spot pretreatment is still mandatory to establish

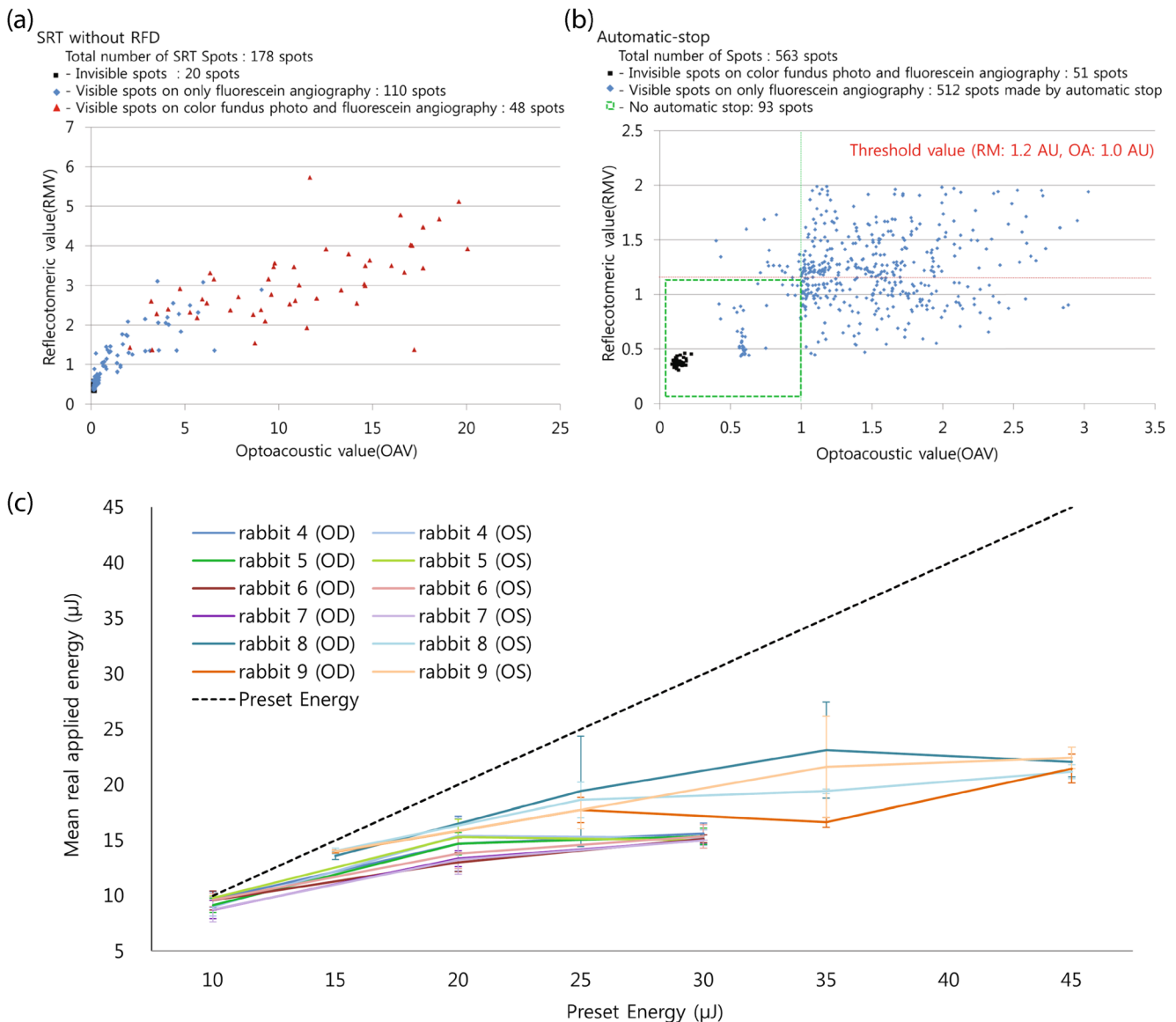


Fig. 8 **a** The optoacoustic value (OAV) and reflectometric value (RMV) from 178 SRT spots by SRT without RFD. The lowest OAV and RMV of 48 visible SRT spots (red arrowhead) are approximately 2.2 AU and 1.4 AU respectively. **b** The OAV and RMV from 563 SRT spots by SRT with RFD. All spots by SRT with RFD did not produce instant

visible spots on CFP. Autostops occurred in 470 of 563 spots. Forty-two of 93 spots with no autostop (inside of green box) induced relatively faint hyperfluorescence on FFA. **c** The mean real-applied pulse energy was lower than the preset pulse energy (10, 15, 20, 25, 30, 35, 45 μ J spots) in 10 eyes of rabbits (nos. 4–9) after SRT with RFD

an adequate pulse energy because of individual variations in threshold energy noted in previous studies [8, 9, 12, 18]. The clinician needs to establish the therapeutic range in individual patients through test spot observation; RFD signals can however support the clinician with an objective value regardless of visibility on FFA and ophthalmoscopy.

In this study, the detection rate of RFD using both OA and RM method was 91.8%, which was lower than the detection rate of 95.7% in previous clinical study [18]. We speculate that the narrower range of pulse energy for rabbit (11–48 μ J) than human (60–200 μ J) in selective RPE damage may have caused the difference. Considering the

accuracy of RFD-va1.1 and no overtreatment after SRT with RFD, determining adequate energy by RFD seems clinically useful to find the therapeutic range of SRT. Besides the threshold of RFD, several factors including defocusing error, media opacity, focal pigmentation, and pathologic conditions like retinal edema and subretinal fluid can affect the feedback signal in real clinical practice [8, 12]. RFD in human subjects has different energy settings and therapeutic thresholds, from RFD-va1.1 in animals. Additional clinical studies are necessary to validate the efficacy of RFD.

In conclusion, RFD-va1.1 showed an effective performance to obtain selective RPE damages without damaging photoreceptors in this study. Therefore, RFD could be useful to titrate the pulse energy for SRT treatment.

Acknowledgements This animal study was supported by the Research Institute of Medical Science of Yeouido St. Mary's hospital.

Funding This study was supported by the grant from South Korean Government's Ministry of Trade, Industry and Energy (M000004912-00192937).

Compliance with ethical standards

Conflict of interest The authors declare that they have no conflict of interest.

Animal ethics All rabbits in this experiment were treated in accordance with the ARVO Statement for the Use of Animals in Ophthalmic and Vision Research, and were approved by the Institutional Animal Care and Use Committee of the Catholic University of Korea.

Disclaimer The sponsor had no role in the design or conduct of this research.

References

- Group TDRSR (1981) Photocoagulation treatment of proliferative diabetic retinopathy. Clinical application of diabetic retinopathy study (DRS) findings, DRS report number 8. *Ophthalmology* 88: 583–600
- group ETDRSr (1985) Photocoagulation for diabetic macular edema. Early treatment diabetic retinopathy study report number 1. *Arch Ophthalmol* 103:1796–1806
- Sivaprasad S, Elagouz M, McHugh D, Shona O, Dorin G (2010) Micropulsed diode laser therapy: evolution and clinical applications. *Surv Ophthalmol* 55:516–530. <https://doi.org/10.1016/j.survophthal.2010.02.005>
- Lim JI (1999) Iatrogenic choroidal neovascularization. *Surv Ophthalmol* 44:95–111
- Schatz H, Madeira D, McDonald HR, Johnson RN (1991) Progressive enlargement of laser scars following grid laser photocoagulation for diffuse diabetic macular edema. *Arch Ophthalmol* 109:1549–1551
- Friberg TR, Karatza EC (1997) The treatment of macular disease using a micropulsed and continuous wave 810-nm diode laser. *Ophthalmology* 104:2030–2038
- Luttrull JK, Musch DC, Mainster MA (2005) Subthreshold diode micropulse photocoagulation for the treatment of clinically significant diabetic macular oedema. *Br J Ophthalmol* 89:74–80. <https://doi.org/10.1136/bjo.2004.051540>
- Park YG, Kim JR, Kang S, Seifert E, Theisen-Kunde D, Brinkmann R, Roh YJ (2016) Safety and efficacy of selective retina therapy (SRT) for the treatment of diabetic macular edema in Korean patients. *Graefes Arch Clin Exp Ophthalmol* 254:1703–1713. <https://doi.org/10.1007/s00417-015-3262-1>
- Roider J, Liew SH, Klatt C, Elsner H, Poerksen E, Hillenkamp J, Brinkmann R, Birngruber R (2010) Selective retina therapy (SRT) for clinically significant diabetic macular edema. *Graefes Arch Clin Exp Ophthalmol* 248:1263–1272. <https://doi.org/10.1007/s00417-010-1356-3>
- Sramek C, Mackanos M, Spitler R, Leung LS, Nomoto H, Contag CH, Palanker D (2011) Non-damaging retinal phototherapy: dynamic range of heat shock protein expression. *Invest Ophthalmol Vis Sci* 52:1780–1787. <https://doi.org/10.1167/iovs.10-5917>
- Brinkmann R, Roider J, Birngruber R (2006) Selective retina therapy (SRT): a review on methods, techniques, preclinical and first clinical results. *Bull Soc Belge Ophtalmol*:51–69
- Kang S, Park YG, Kim JR, Seifert E, Theisen-Kunde D, Brinkmann R, Roh YJ (2016) Selective retina therapy in patients with chronic central serous chorioretinopathy: a pilot study. *Medicine (Baltimore)* 95:e2524. <https://doi.org/10.1097/md.0000000000002524>
- Kim HD, Han JW, Ohn YH, Brinkmann R, Park TK (2014) Functional evaluation using multifocal electroretinogram after selective retina therapy with a microsecond-pulsed laser. *Invest Ophthalmol Vis Sci* 56:122–131. <https://doi.org/10.1167/iovs.14-15132>
- Park YG, Kang S, Brinkmann R, Roh YJ (2015) A comparative study of retinal function in rabbits after panretinal selective retina therapy versus conventional panretinal photocoagulation. *J Ophthalmol* 2015:247259. <https://doi.org/10.1155/2015/247259>
- Lavinsky D, Sramek C, Wang J, Huie P, Dalal R, Mandel Y, Palanker D (2014) Subvisible retinal laser therapy: titration algorithm and tissue response. *Retina* 34:87–97. <https://doi.org/10.1097/IAE.0b013e3182993edc>
- Schuele G, Elsner H, Framme C, Roider J, Birngruber R, Brinkmann R (2005) Optoacoustic real-time dosimetry for selective retina treatment. *J Biomed Opt* 10:064022. <https://doi.org/10.1117/1.2136327>
- Park YG, Seifert E, Roh YJ, Theisen-Kunde D, Kang S, Brinkmann R (2014) Tissue response of selective retina therapy by means of a feedback-controlled energy ramping mode. *Clin Exp Ophthalmol* 42:846–855. <https://doi.org/10.1111/ceo.12342>
- Park YG, Kang S, Kim M, Yoo N, Roh YJ (2017) Selective retina therapy with automatic real-time feedback-controlled dosimetry for chronic central serous chorioretinopathy in Korean patients. *Graefes Arch Clin Exp Ophthalmol* 255:1375–1383. <https://doi.org/10.1007/s00417-017-3672-3>
- Vujosevic S, Martini F, Longhin E, Convento E, Cavarzeran F, Midena E (2015) Subthreshold micropulse yellow laser versus subthreshold micropulse infrared laser in center-involving diabetic macular edema: morphologic and functional safety. *Retina* 35: 1594–1603. <https://doi.org/10.1097/iae.0000000000000521>
- Framme C, Schuele G, Roider J, Kracht D, Birngruber R, Brinkmann R (2002) Threshold determinations for selective retinal pigment epithelium damage with repetitive pulsed microsecond laser systems in rabbits. *Ophthalmic Surg Lasers* 33:400–409